

## Water Resources Research

### RESEARCH ARTICLE

10.1029/2018WR023080

#### Key Points:

- Tree ring reconstructions of streamflow in the Upper Indus Basin show wetter conditions in the 1990s compared to the last 600 years
- Reconstructions are insensitive to the choice of statistical method used (principal components versus Bayesian regression)
- Streamflow is most sensitive to winter precipitation and summer temperature, but anomalies in these seasons cannot explain recent high flow

#### Supporting Information:

- Supporting information S1
- Data Set S1
- Data Set S2

#### Correspondence to:

M. P. Rao,  
mukund@ldeo.columbia.edu

#### Citation:






Rao, M. P., Cook, E. R., Cook, B. I., Palmer, J. G., Uriarte, M., Devineni, N., et al. (2018). Six centuries of Upper Indus Basin streamflow variability and its climatic drivers. *Water Resources Research*, 54. <https://doi.org/10.1029/2018WR023080>

Received 8 APR 2018

Accepted 27 JUL 2018

Accepted article online 3 AUG 2018

## Six Centuries of Upper Indus Basin Streamflow Variability and Its Climatic Drivers

Mukund Palat Rao<sup>1,2</sup> , Edward R. Cook<sup>1</sup> , Benjamin I. Cook<sup>3,4</sup> , Jonathan G. Palmer<sup>5</sup> , Maria Uriarte<sup>6</sup>, Naresh Devineni<sup>7,8</sup> , Upmanu Lall<sup>8,9</sup> , Rosanne D. D'Arrigo<sup>1</sup>, Connie A. Woodhouse<sup>10</sup> , Moinuddin Ahmed<sup>11</sup>, Muhammad Usama Zafar<sup>11</sup>, Nasrullah Khan<sup>12</sup>, Adam Khan<sup>11</sup>, and Muhammad Wahab<sup>13</sup>

<sup>1</sup>Tree Ring Laboratory, Lamont-Doherty Earth Observatory, Columbia University, Palisades, NY, USA, <sup>2</sup>Department of Earth and Environmental Science, Columbia University, New York, NY, USA, <sup>3</sup>NASA Goddard Institute for Space Studies, New York, NY, USA, <sup>4</sup>Ocean and Climate Physics, Lamont-Doherty Earth Observatory, Columbia University, Palisades, NY, USA, <sup>5</sup>ARC Centre of Excellence in Australian Biodiversity and Heritage, School of Biological, Earth and Environmental Sciences, University of New South Wales, Sydney, New South Wales, Australia, <sup>6</sup>Ecology, Evolution, and Environmental Biology, Columbia University, New York, NY, USA, <sup>7</sup>Department of Civil Engineering, The City College of New York, New York, NY, USA, <sup>8</sup>Columbia Water Center, Columbia University, New York, NY, USA, <sup>9</sup>Department of Earth and Environmental Engineering, Columbia University, New York, NY, USA, <sup>10</sup>School of Geography and Development, University of Arizona, Tucson, AZ, USA, <sup>11</sup>Dr. Moinuddin Ahmed Laboratory of Dendrochronology and Plant Ecology, Botany Department, Federal Urdu University of Arts Science and Technology, Karachi, Pakistan, <sup>12</sup>Laboratory of Plant Ecology, Department of Botany, University of Malakand, Chakdara, Pakistan, <sup>13</sup>Botany Department, Women University Swabi, Swabi, Pakistan

**Abstract** Our understanding of the full range of natural variability in streamflow, including how modern flow compares to the past, is poorly understood for the Upper Indus Basin because of short instrumental gauge records. To help address this challenge, we use Hierarchical Bayesian Regression with partial pooling to develop six centuries long (1394–2008 CE) streamflow reconstructions at three Upper Indus Basin gauges (Doyian, Gilgit, and Kachora), concurrently demonstrating that Hierarchical Bayesian Regression can be used to reconstruct short records with interspersed missing data. At one gauge (Partab Bridge), with a longer instrumental record (47 years), we develop reconstructions using both Bayesian regression and the more conventionally used principal components regression. The reconstructions produced by principal components regression and Bayesian regression at Partab Bridge are nearly identical and yield comparable reconstruction skill statistics, highlighting that the resulting tree ring reconstruction of streamflow is not dependent on the choice of statistical method. Reconstructions at all four reconstructions indicate that flow levels in the 1990s were higher than mean flow for the past six centuries. While streamflow appears most sensitive to accumulated winter (January–March) precipitation and summer (May–September) temperature, with warm summers contributing to high flow through increased melt of snow and glaciers, shifts in winter precipitation and summer temperatures cannot explain the anomalously high flow during the 1990s. Regardless, the sensitivity of streamflow to summer temperatures suggests that projected warming may increase streamflow in coming decades, though long-term water risk will additionally depend on changes in snowfall and glacial mass balance.

### 1. Introduction

The Indus River and its tributaries provide the main source of water for Pakistan's vast irrigation network and hydropower generation for its power grid in an otherwise arid to semiarid country. The river basin consists of seven main rivers, the Indus, Kabul, Jhelum, and Chenab, known collectively as the western tributaries, and the Beas, Ravi, and Sutlej known as the eastern tributaries (Zawahri, 2009). Of these, the Indus is the most important as it contributes close to half of the overall discharge of the basin. The Indus River Basin is typically divided into two sections, the Upper Indus Basin (UIB) and Lower Indus Basin. The UIB refers to the section of the river above the Tarbela reservoir, an important source of water for Pakistan's irrigation network and hydropower potential (Rashid et al., 2018), and located on the main Indus before its confluence with other major tributaries (Archer, 2003). The headwaters of the UIB originate in the upper reaches of the Karakoram and Himalaya ranges. Approximately three fourths of UIB discharge is estimated to be a result of melting snow and ice, while summer rainfall plays a smaller role in contributing to the total discharge (Immerzeel et al., 2009). The interannual variability in UIB discharge is largely controlled by variability in

the ablation of glacial mass balance and seasonal snowfall (Forsythe et al., 2017). Consequently, future changes in UIB flow will likely be regulated by changes in glacial mass balance and seasonal snowfall and the melt rate of both of these components. These melt rates are primarily controlled by changes in temperature and humidity (Harpold & Brooks, 2018; Immerzeel et al., 2010). Overall, for the Indus Basin (Lower Indus Basin and UIB) climate model projections of future runoff exhibit high uncertainty due to a large spread in precipitation (winter and summer) projections (Ali et al., 2015; Immerzeel et al., 2013; Lutz et al., 2016). However, there is a broad consensus that as glaciers recede, annual glacial runoff volume will likely increase until a maximum point known as *peak water*, beyond which runoff will decrease due to the reduced glacial area becoming unable to sustain the same runoff (Huss & Hock, 2018; Lutz et al., 2014). Future water management strategies (e.g., at the Tarbela reservoir) will therefore naturally depend on expected changes in UIB discharge (Tahir et al., 2011).

Conflicting interpretations of recent climate and glacier trends have been observed over the high ranges of the Karakoram Mountains. While glaciers have declined over much of the Himalayas, glaciers in the Karakoram have either remained stable or even expanded in certain cases (Bolch et al., 2012; Brun et al., 2017; Gardelle et al., 2012; Kapnick et al., 2014; Minora et al., 2013). This anomalous behavior of glaciers has been referred to as the *Karakoram Anomaly* (Hewitt, 2005). Two-thirds of high-altitude snow over the Karakoram accumulates in the winter, and is caused by synoptic westerly disturbances, while the remainder is attributed to monsoonal influences (Benn & Owen, 1998; Greene & Robertson, 2017; Palazzi et al., 2015). While the underlying causes of the Karakoram Anomaly remain unclear, it has been attributed to increases in summertime cloudiness (Bashir et al., 2017; Hewitt, 2005; Zafar et al., 2015), decreasing summertime temperature (Fowler & Archer, 2006), increases in wintertime snowfall (Farhan et al., 2015; Kapnick et al., 2014; Ridley et al., 2013; Tahir et al., 2011), high debris loading on the glaciers that insulates the underlying glaciers (Kraaijenbrink et al., 2017; Minora et al., 2013), land surface feedbacks due to intensified lowland irrigation (de Kok et al., 2018), and a southward shifted summertime westerly jet (Forsythe et al., 2017).

Our understanding of recent streamflow trends, if any, is to a large extent limited by the short instrumental streamflow discharge records in the region that extend back two to four decades at the longest. Having such short instrumental records encumbers our understanding of the full range of natural variability, especially at decadal to centennial time scales, and cannot provide a sufficient long-term context to assess possible recent changes in discharge. Predictions of future water risk may also be improved by a better understanding of the current and past variability and climatic controls of discharge (Archer et al., 2010; Forsythe et al., 2017; Lutz et al., 2014).

To help address these multiple challenges, we present three new and one updated (cf. Cook et al., 2013) reconstruction of UIB discharge at four discharge gauging stations (Partab Bridge, Doyian, Gilgit, and Kachora) for the past six centuries. These paleohydrologic reconstructions are developed using annually resolved climatically sensitive tree ring chronologies in the UIB (Figure 1). These longer-term estimates of past flow can be used to better assess recent trends in UIB streamflow. Due to the constraints of sparse instrumental discharge data at the three shorter gauge records (Doyian, Gilgit, and Kachora) we develop reconstructions using Hierarchical Bayesian Regression (HBR) with partial pooling (Devineni et al., 2013). At one gauge with a long instrumental record (Partab Bridge) we test two reconstruction methods, Bayesian regression (BR) and principal components regression (PCR, see section 3). The motivation behind developing a reconstruction using both PCR and BR at the same target gauge (Partab Bridge) from the same tree ring predictor network is to test the hypothesis that streamflow reconstructions and their uncertainties should be highly comparable notwithstanding of the choice of statistical methodology used. The objectives of this are twofold. First, this provides a useful foundation upon which to base the choice of statistical methodology (i.e., PCR vs BR) for future reconstructions of streamflow or climate. Second, it allows us to compare the newly developed HBR reconstructions of streamflow at the three streamflow gauge records (Doyian, Gilgit, and Kachora) against the reconstruction developed at Partab Bridge (cf. Cook et al., 2013). We then investigate the potential climate drivers of streamflow at the four gauges for which we develop reconstructions of past discharge, along with the climate drivers of annual growth for the suite of tree ring predictors used in our reconstruction model. We hypothesize that if the trees show a similar growth response to climate as the streamflow response to climate, then that provides additional evidence that the paleo-discharge estimates presented here were caused by the same climatic forcing. Finally, the climate analyses allow us to specifically test how climate may have contributed to the high discharge rates in the 1990s and declining flows in the

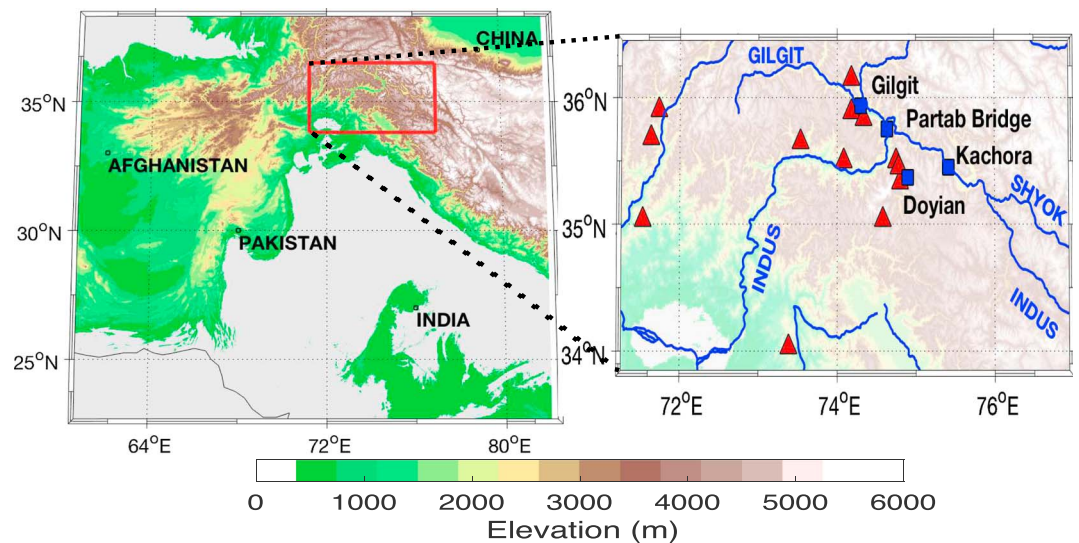


**Figure 1.** Map showing locations of streamflow gauges (blue squares) and tree ring sites (red triangles) used in this study. The red box in the figure on the left highlights the region for which a close-up is shown on the right.

early 2000s (Cook et al., 2013; Forsythe et al., 2017; Hasson et al., 2017). Taken together, we believe that the four long-term reconstructions of past discharge, along with the streamflow climate and tree growth climate response analysis, provide a useful framework and context to better predict UIB hydrological regime changes.

## 2. Data

### 2.1. Instrumental Streamflow and Climate Data

Instrumental streamflow data were obtained from the Pakistan Water and Power Development Authority at the four target gauges, Partab Bridge, Doyian, Gilgit, and Kachora (Figure 1). Mean annual (January–December) discharge at each of these gauges is shown in Figure 2, and Table 1 describes some additional characteristics of the data (e.g., sub-basin names, mean, and standard deviation). The instrumental record for Partab Bridge was updated to 2008 (dashed line Figure 2) using estimates from three other gauges (Dainyor, Gilgit, and Kachora) as described in Cook et al. (2013). The data quality in early part of the Gilgit

record between 1960 and 1972 exhibits greatly reduced interannual variability compared to the later part of the record. Consequently, we assume this to be a data quality issue and disregard the early period of the Gilgit data in subsequent analysis. Discharge at the gauges peaks between May and September as seen in the monthly discharge hydrograph (Figure 3). We obtained temperature and precipitation data from the global gridded 0.5° resolution Climatic Research Unit Time Series v.4.01 data set that covers the period 1901–2016. A box plot of monthly climate (temperature and precipitation) averaged across a 2° latitude × 2° longitude grid (73.5–75.5°E and 34.5°N–36.5°N) between 1961 and 2016 is also shown in Figure 3. These 2° × 2° regionally averaged temperature and precipitation series are used in the climate analyses with streamflow and tree growth.

### 2.2. Tree Ring Network

The annual growth of trees is often controlled on interannual and decadal time scales by the same climatic factors that control streamflow in rivers (Meko et al., 1995). These may include winter snowpack and summer temperatures (e.g., Woodhouse & Lukas, 2006), summer drought (e.g., Cook & Jacoby, 1983; Devineni et al., 2013), and monsoonal

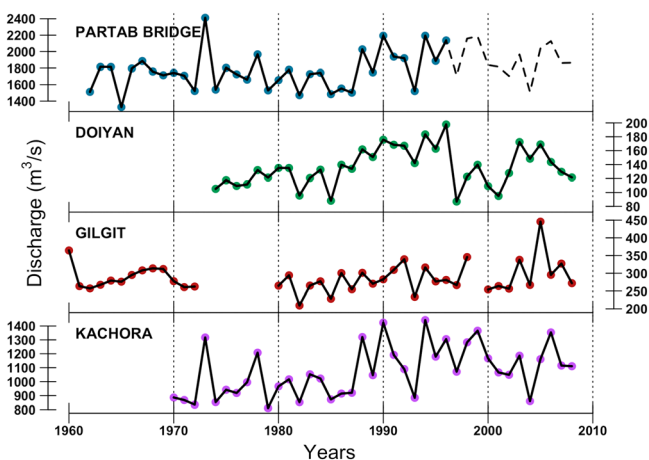


**Figure 2.** Instrumental period mean annual discharge ( $m^3/s$ ) at four streamflow gauges in the Upper Indus Basin watershed (solid black). The Partab Bridge record between 1997 and 2008 (dashed line) is estimated by using three proximal streamflow gauges (Cook et al., 2013).

**Table 1**  
Streamflow Gauge Network in the Upper Indus Basin

Gauge	River (sub-basin)	Lat.	Lon.	Elev. (m)	Start	End	Missing data	Annual mean (m <sup>3</sup> /s)	SD (m <sup>3</sup> /s)	Skewness
Partab Bridge	Indus	35.78	74.63	1419	1962	1996	-	1763.43	237.34	0.66
Doyian	Astore	35.33	76.42	1195	1974	2008	-	135.79	27.79	0.21
Gilgit	Gilgit	35.11	74.06	1140	1960 <sup>a</sup> –1980	2008	1973–1979, Jul–Dec 1999	286.99	45.50	1.44
Kachora	Indus	35.27	75.25	1460	1970	2008	-	1074.85	181.79	0.38

Note. SD = standard deviation.

<sup>a</sup>We only use the 1980–2008 section of the Gilgit gauge record for ensuing analysis.

precipitation (e.g., D'Arrigo et al., 2011). This underlying principle has allowed the use tree rings to develop reconstructions of past flow and flow extremes, including for one gauge on the UIB (Cook et al., 2013). These paleohydrologic records from tree rings have found a wide variety of applications, from placing instrumental mean discharge in a long-term context (Stockton & Jacoby, 1976); to being used as forecasting, planning, and research tools by water managers (Meko & Woodhouse, 2011); and understanding continental-scale streamflow covariability and clustering (Ho et al., 2017).

For our study, as an initial screening for useful tree ring predictors to develop our streamflow reconstruction models we downloaded all tree ring series located within the broad Karakoram and Western Himalaya region with an end year later than 2005 from the International Tree Ring Data Bank (<https://www.ncdc.noaa.gov/data-access/paleoclimatology-data/datasets/tree-ring>). The raw annual ring-width data for each site were *standardized* (Cook & Kairiukstis, 1990; Fritts, 1976) using the *signal-free* method (Melvin & Briffa, 2008). The signal-free method aims to maximize the preservation of common medium frequency variance in tree ring series and eliminate trend distortion effects with attention paid to preserving multidecadal to centennial variability due to climate. A series was retained as a predictor in a model if it is correlated at  $p < 0.05$  using a two-sided  $t$  test with the streamflow gauge record. Tree ring series were also tested as potential predictors with a lag of 1 year (lag  $t + 1$ ) with respect to the streamflow data, as often prior year climate can influence current year tree growth (Fritts, 1976). In our analyses, we develop two sets of models. The first is a reconstruction of May through September (MJJAS) flow at Partab Bridge using two reconstruction methods, PCR and BR (Model I). The second is a HBR reconstruction of annual (January–December) flow at Doyian, Gilgit, and Kachora (Model II). The choice of the MJJAS season at the target for the reconstruction at Partab

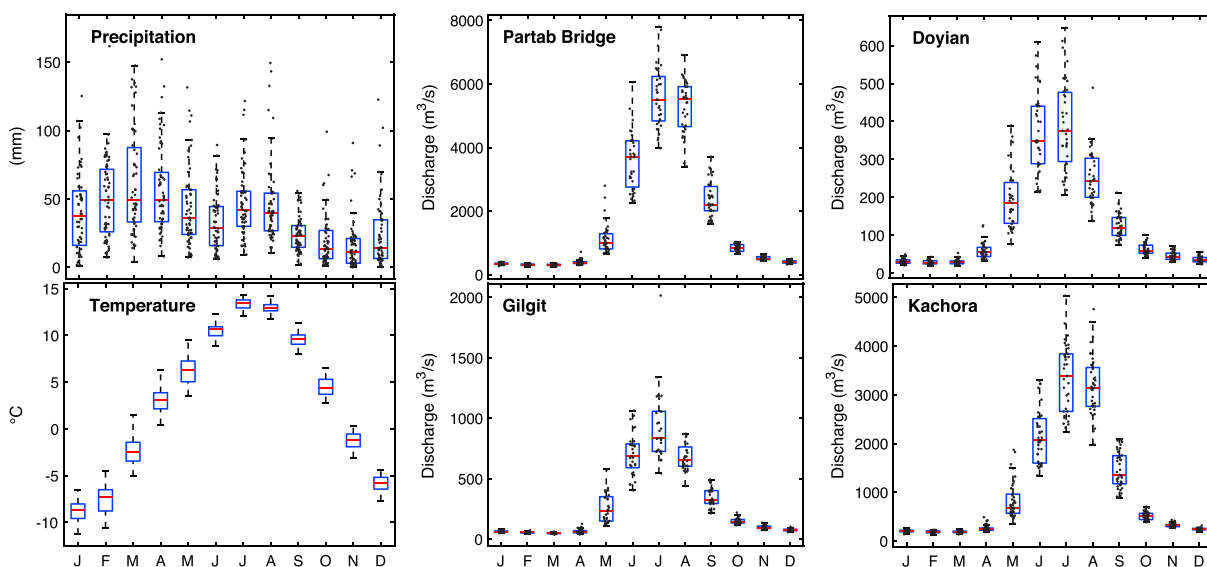


**Figure 3.** Boxplots showing month-by-month variability in precipitation (mm) and temperature (°C) between 1961 and 2016, and monthly discharge hydrographs (m<sup>3</sup>/s) for the instrumental period at four streamflow gauges in the UIB. Note the different y axis ranges. X axis labels represent months of the year. UIB = Upper Indus Basin.

Bridge is that it coincides with the peak flow season (cf. Cook et al., 2013). For the HBR reconstructions of flow at Doyian, Gilgit, and Kachora, we first attempted to develop MJJAS season streamflow reconstructions as well, followed by a Northern Hemisphere water-year (October–September) reconstruction. However, these two models performed poorly compared to a model reconstructing mean annual (January–December) discharge based on their calibration-validation statistics (see section 3). Based on our predictor screening criteria we use 15 tree ring series as predictors for the reconstruction model at Partab Bridge and 10 series as predictors for the HBR reconstruction model at the other 3 gauges. The final set of predictor tree ring series used in Models I and II is shown in Table S1 and plotted in Figure S2 in the supporting information (Bunn, 2010). The original source for these collections are Ahmed et al. (2011), Ahmed et al. (2013), and Zafar et al. (2010).

### 3. Methods

#### 3.1. Reconstruction Model

A commonly used method to reconstruct a predictand (or dependent) variable such as streamflow or climate from tree rings is principal components regression (PCR, Cook et al., 2010, 1999, 2013; Harley et al., 2017; Harley & Maxwell, 2017). However, PCR cannot be easily used to reconstruct streamflow at gauges that have extremely short records and data gaps, without an imputation step for the missing data. For the UIB specifically, while the length of each available gauge record is relatively short (Figure 2), we are fortunate to have a network of gauging stations that are in close proximity to each other and located on different tributaries in the same watershed (Figure 1 and Table 1). An alternative streamflow reconstruction method to PCR is HBR with partial pooling (e.g., Devineni et al., 2013). HBR with partial pooling allows regression coefficients to be correlated across the gauges being reconstructed by modeling the vector of regression coefficients as draws from a common multivariate normal distribution. The physical basis of this assumption is that streamflow discharge tends to be correlated at the scale of a watershed (Figure S1, Ho et al., 2017). This partial pooling framework allows us to shrink the number of free parameters to be estimated and reconstruct streamflow at gauges with short instrumental records. This can result in lower uncertainty in estimated parameters and reconstructed discharge, along with improving the skill of the final model by combining the regression strength of the model across gauges (Devineni et al., 2013). Finally, HBR estimates predicted values by drawing from prior distributions and can therefore handle data gaps in a very natural way.

For the UIB, Cook et al. (2013) used PCR to reconstruct May through September (MJJAS) peak season discharge at Partab Bridge between 1452 and 2008 CE. Partab Bridge was chosen as the target gauge for reconstruction by Cook et al. (2013) because it has the longest continuous available record of flow and also includes discharge from both the east and west regions of the UIB (Figure 1). We develop PCR and BR models at Partab Bridge to produce a slightly longer reconstruction (cf. Cook et al., 2013) between 1430 and 2008 CE (originally 1452–2008 CE). The original Cook et al., 2013 PCR reconstruction at Partab Bridge and the one produced and developed here are identical over the period of overlap between 1452 and 2008 CE. In all reconstructions we used a multiple linear regression framework where we estimated streamflow (the predictand variable) using a vector of predictor variables. The vectors of predictor variables used are the principal component (PC) scores (Cooley & Lohnes, 1971) of the suite of normalized tree ring-width indices (RWI). The RWI were normalized using their respective calibration period means and standard deviations, and the PCs were computed from the RWI suite to be orthogonal during the calibration period (Cook et al., 1999). In each model, only leading PCs with eigenvalues greater than 1 were retained as potential predictors for streamflow as an estimate of common shared *signal* (versus noise) across the different tree ring series using the Kaiser-Guttman criteria (Guttman, 1954; Kaiser, 1960). We used a *nested* approach in both Models I and II, where shorter tree ring predictor series were dropped sequentially until the predictor suite was exhausted and reconstructions were made for each nest (e.g., Meko, 1997). To develop the final nested reconstruction, we appended each longer nest to the start year of the shorter nest after scaling its variance to that of the calibration period instrumental data.

For the reconstruction at Partab Bridge using PCR and BR (Model I) we used a 30-year period between 1975 and 2004 as a model calibration period and the early part of the data between 1962 and 1974 (13 years) as the model validation period. This is the same calibration and validation period used in Cook et al. (2013). For the HBR models at Doyian, Gilgit, and Kachora (Model II) we used a 1970–2004 calibration period with a leave-one-out cross-validation (LOOCV) approach to compute model validation statistics. LOOCV was used for

the HBR model as the individual instrumental time series were too short to divide into separate calibration and validation periods. After accounting for the varying start years of the gauge records (Table 1) the length of the calibration periods for Model II were as follows: Doyian ( $n = 29$ ), Gilgit ( $n = 23$ ), and Kachora ( $n = 33$ ). The longer Partab Bridge record was not included in the HBR reconstruction (Model II) to maintain the independence between the predictand variables (i.e., the streamflow gauge) being reconstructed, as the Partab Bridge record between 1997 and 2008 was estimated by Cook et al., 2013 using the Gilgit and Kachora records. We used the Shapiro-Wilk normality test (Shapiro & Wilk, 1965) to test the null hypothesis that the streamflow data come from normal distributions. For instrumental MJJAS flow at Partab Bridge and annual flows at Doyian and Kachora we accepted this null hypothesis of normality, while at Gilgit we rejected the null hypothesis that annual flow is normally distributed at  $p < 0.05$ . However, after examining the kernel density plot (not shown) and time series plot of mean annual streamflow at Gilgit (Figure 2), we found that if the high flow anomaly in 2005 is excluded, then the skewness decreases from 1.44 to 0.14, and we would have accepted the null hypothesis of streamflow being normally distributed at Gilgit. When testing for normality during the calibration period (1975–2004, Partab Bridge; 1970–2004, Doyian, Gilgit, and Kachora) at all three gauges, we accepted the null hypothesis of normality. Therefore, we chose to not transform (e.g., log or power transform) the original data at Gilgit in our streamflow reconstruction. This was also done to retain the same units across the three gauges being reconstructed using HBR. Prior to developing the PCR, BR, HBR models, the streamflow data were also normalized by subtracting their respective calibration period means and dividing their respective calibration period standard deviations. The final reconstructions were then scaled to the calibration period mean and variance.

We tested model calibration and validation fidelity by computing the following statistics: (i) CRSQ (calibration period coefficient of multiple determination or  $R^2$ ), (ii) CVRE (calibration period reduction of error calculated by LOOCV), (iii) VRSQ (validation period square of the Pearson correlation or  $r^2$ ), (iv) VRE (validation period reduction of error), and (v) VCE (validation period coefficient of efficiency, see supporting information in Cook et al., 2010). The VCE is equivalent to the Nash-Sutcliffe efficiency test (Nash & Sutcliffe, 1970). For the HBR model, we only present CRSQ, CVRE, and RE (reduction of error) statistics as the model does not have a formal validation period due to the shortness of the gauge records. The formulation used for calculating RE for the HBR model is as follows:

$$RE = 1 - \frac{SSE_v}{SSE_{null}}$$

where  $SSE_v$  is the sum of squares of cross-validation errors and  $SSE_{null}$  is the sum of squares of differences using the calibration mean as the prediction for each year (Meko, 2006). In general, models with VRE, VCE, and RE values greater than 0 are considered an indication that the model has skill compared to using the calibration period, validation period, and calibration period means, respectively, as the estimate for each year. We also compared model performance using median-normalized root-mean-square error (RMSE) (Janssen & Heuberger, 1995) statistic calculated as

$$RMSE = \sqrt{\frac{1}{n} \sum_{t=1:n} (y_t - \hat{y}_t)^2}$$

$$\text{median-normalized RMSE} = 100 \frac{RMSE}{\text{median}(y_t)}$$

where  $y_t$  and  $\hat{y}_t$  are the observed and predicted discharge in year  $t$ , respectively. The median-normalized RMSE can be thought to represent how large the model error is as a percentage of the median discharge, with larger values representing larger error.

### 3.1.1. Principal Components Regression

PCR is used here to reconstruct streamflow discharge from tree rings and is the same method used to reconstruct UIB discharge at Partab Bridge by Cook et al. (2013). Following that work, we also estimated model uncertainties in PCR by applying maximum entropy bootstrapping ( $n = 300$ ; MEBoot, Vinod, 2006; Vinod & López-de-Lacalle, 2009) to both the tree ring and streamflow data. MEBoot can be thought of here as a random perturbation method that is applied to both the predictor and predictand series. In so doing, MEBoot preserves the overall stochastic properties of the original time series used in regression line the chronological order of the data being resampled, but changes in a random fashion the PCs derived from the PCR procedure,

along with the streamflow data. As such, the MEBoot procedure also produces an empirical probability distribution functions for each reconstructed year that contributes to the uncertainty estimates on the reconstructions (Cook et al., 2013).

### 3.1.2. Bayesian Regression

#### 3.1.2.1. HBR With Partial Pooling

$$y_{i,t}|\alpha_i, \beta_i = \alpha_i + \beta_i * X_t + \varepsilon_{i,t} (i = 1, 2, 3)$$

$$\beta_i \sim \text{MVN}(\mu_B, \Sigma_B)$$

Priors modeled as

$$\alpha_i \sim N(0, 10^4)$$

$$\varepsilon_{i,t} \sim N(0, 10^4)$$

$$\mu_B \sim \text{MVN}(0, 10^4 I)$$

$$\Sigma_B \sim \text{Inv - Wishart}_{v_0}(A_0)$$

HBR reconstructions with partial pooling were developed at each gauge using a multiple linear regression of streamflow ( $y_{i,t}$ ) at gauge  $i$  at year  $t$  on a vector of predictors ( $X_t$ ). The matrix  $\mathbf{X}$  contains the PC score time series of tree ring predictors used in the current nest.  $\beta_i$  is a vector of the corresponding regression slopes for each predictor in the vector  $X_t$  at gauge  $i$ . Each regression includes an intercept term  $\alpha_i$  and a prediction error term  $\varepsilon_{i,t}$ . We modeled priors to be vague or noninformative (Gelman & Hill, 2006) and the covariance structure of regression coefficients  $\beta_i$  for each streamflow gauge to be derived from a multivariate normal distributions (MVN). This assumption is based on the consideration that annual flows are correlated across gauges (Figure S1). Parameter  $\beta_i$  is in turn described by two hyperparameters  $\mu_B$  and a dispersion matrix  $\Sigma_B$  leading to the hierarchical framework in our model (Gelman & Hill, 2006). We assumed the prior for covariance matrices  $\Sigma_B$  to be an inverse Wishart distribution with scale matrix  $A_0$ , specified to be an identity matrix  $I$  with  $v_0$  degrees of freedom (Devineni et al., 2013).  $v_0$  is set to be one more than the dimension of the matrix or the total number of predictors used in the nest.

We hypothesize that by modeling the covariance structure of regression coefficients we are able to borrow the strength of the regression estimates at one streamflow gauge and use that for predictions at another gauge (Devineni et al., 2013). This permits us to derive a better regression estimates during the model calibration period and consequently makes a better prediction of past streamflow. Unlike in Devineni et al. (2013), here we modeled the associated prediction error terms, or residuals,  $\varepsilon_{i,t}$  be derived from a normal distribution and not from a MVN. This is because each streamflow gauge discharge series spans a different range of years (Figure 2). Consequently, it was not possible to compute the spatial covariance of the error term. Also, our matrix  $\mathbf{X}$  uses PC scores and not the standardized tree ring series directly (cf. Devineni et al., 2013). This predictand *data reduction* was necessary due to shortness of the gauge records, to reduce the number of *free parameters* to be estimated relative to the number of years of streamflow data available for model calibration.

The final joint posterior distribution  $\mathbf{P}(\theta|\mathbf{y})$  for the partial pooling case, with regression intercepts  $\alpha_i$ , slopes  $\beta_i$ , error  $\varepsilon_{i,t}$ , and covariance  $\Sigma_B$ , is described as follows.

$$\mathbf{P}(\theta|\mathbf{y}) \propto \prod_{i=1}^3 \prod_{t=1}^{n_t} [N(y_i(t)|\alpha_i + \beta_i X(t), \varepsilon_i(t))] * N(\alpha_i|0, 10^4)$$

$$\text{MVN}(\beta_i|\mu_B, \Sigma_B) * \text{Inv-Wishart}(\Sigma_B|V_0, A_0)$$

$$\text{MVN}(\mu_B|0, 10^4 I) * N(\varepsilon_i(t)|0, 10^4)$$

For each model we estimated the parameters  $\theta$  and the posterior distributions  $\mathbf{P}(\theta|\mathbf{y})$  by employing a Gibbs sampler, a Markov Chain Monte Carlo method using the software Just Another Gibbs Sampler (Plummer, 2003). We simulated three chains, where the parameters were assigned random starting values. This was done to test whether starting values affect convergence toward the final parameter estimates. The chains were run for a 1,000-cycle burn-in to discard the initial state of parameter estimates following which we ran 10,000 simulations. We determined the chains to have converged by visually analyzing the trace plots for the parameters and checking whether the Gelman-Rubin diagnostic shrink factors were less than 1.1

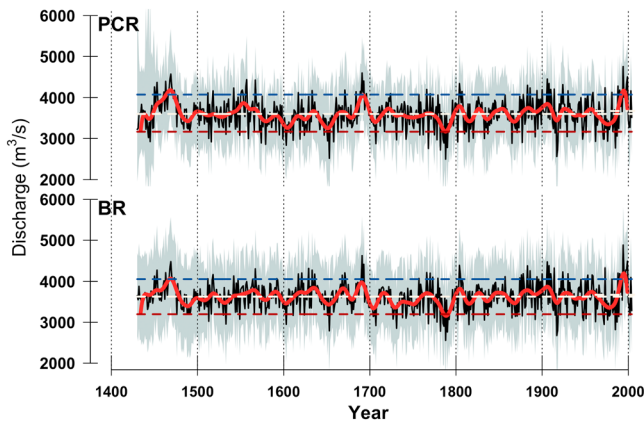


**Figure 4.** Reconstructed mean May through September (MJJAS) discharge ( $\text{m}^3/\text{s}$ ) at Partab Bridge 1430–2008 CE (solid black) using principal components regression (PCR) and Bayesian regression (BR) along with 20-year low-pass filtered reconstruction (solid red). Horizontal dashed red and blue lines are 5th and 95th percentiles of the reconstructions, respectively. The horizontal white line between 1400 and 2008 CE represents the mean of the full reconstruction, and that between 1962 and 2008 CE is the mean of the instrumental period. CE = Common Era.

(Gelman & Rubin, 1992). To validate the fit of our model, we computed the Bayesian  $p$  values for the mean and sum of squared errors (SSQ). The Bayesian  $p$  value for the mean and SSQ were calculated as the proportion of times the mean and SSQ of the model simulated calibration, and validation data were greater than that of the actual streamflow data. A Bayesian  $p$  value of close to 0.50 indicates good model fit. The final reconstructions and our Just Another Gibbs Sampler code are available in Data Sets S1 and S2, respectively.

### 3.1.2.2. Bayesian Regression

While the relatively more complex HBR model was used to reconstruct multiple gauges simultaneously (Doyian, Gilgit, and Kachora), we developed a simplified BR model to reconstruct streamflow at Partab Bridge for comparison with the PCR reconstruction. Unlike the HBR model, the BR model has no hierarchy, as only one gauge is being reconstructed. In this model, we assumed the regression slopes  $\beta_i$  to be derived from a normal distribution. Two sets of BR models were used to develop flow estimates at Partab Bridge. The first is a model that uses tree ring predictors, and the resulting reconstruction from it was then used for the comparison with the streamflow reconstruction developed using PCR. In the second model, we use our analysis of the climatic controls of streamflow at Partab Bridge to develop estimates of streamflow between 2009 and 2016.

## 4. Results

### 4.1. Streamflow Reconstructions

The MJJAS seasonal reconstruction of streamflow at Partab Bridge (Figure 4) and the three HBR reconstructions of mean annual streamflow at Doyian, Gilgit, and Kachora (Figure 5) all indicate that the period of decadal high flow between 1991 and 2000 is unusual in the long-term context of the past six centuries. The only comparable period of high flow in the reconstructions occurs during the 1470s. In all reconstructions, the 20-year low-pass filtered discharge exceeds the 90th percentile of reconstructed discharge over the past six centuries (but remains within reconstruction uncertainties), indicated by the dashed blue horizontal lines. Following this peak in the 1990s, both the instrumental data and reconstructions suggest a decrease in discharge post-2000. Periods of anomalous low flow are indicated in the MJJAS seasonal

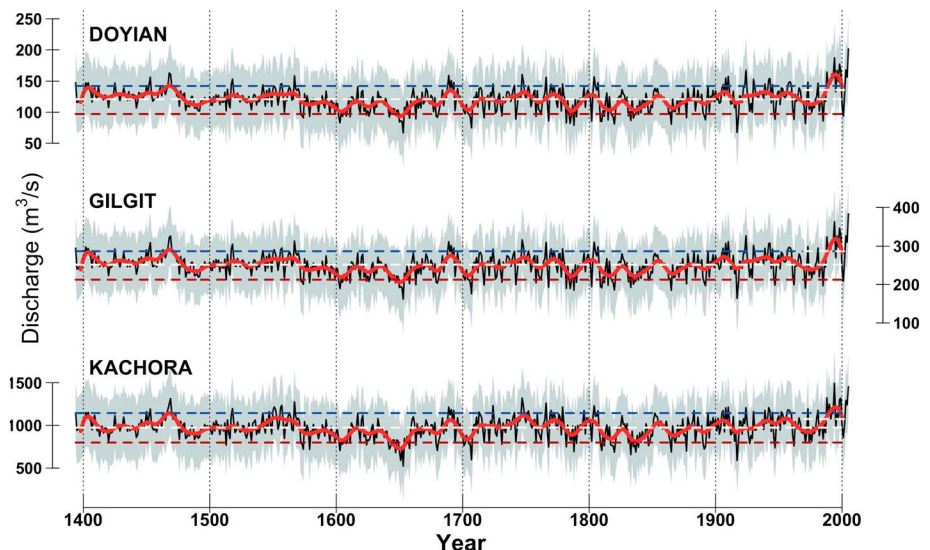


**Figure 5.** Same as Figure 4 but showing reconstructed mean annual (January–December) flow ( $\text{m}^3/\text{s}$ ) at Doyian, Gilgit, and Kachora between 1394 and 2008 CE using Hierarchical Bayesian Regression with partial pooling. CE = Common Era.



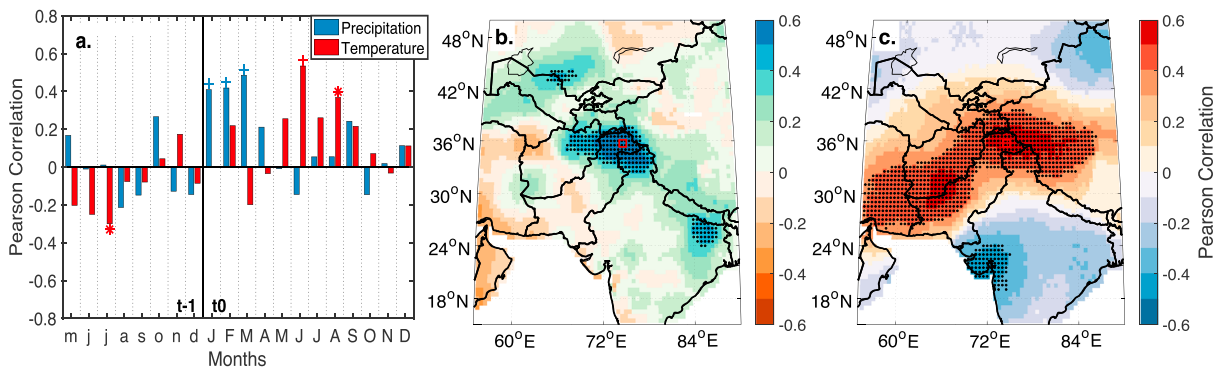


**Figure 6.** Pearson's correlations between MJJAS mean discharge at Partab Bridge (1962–2008) and (a) month-by-month precipitation (blue) and temperature (red; \*,  $p < 0.05$  and +,  $p < 0.01$ ) for months between prior year ( $t - 1$ ) May through current year ( $t_0$ ) December, (b) January–March (JFM) mean precipitation (positive-green; negative-red), and (c) MJJAS mean temperature (positive red and negative blue). All time series were computed as first differences. In Figures 6b and 6c stippling indicates significance at  $p < 0.01$ , while the red square is the location of the gauge station. MJJAS = May–September.

reconstruction at Partab Bridge in the early 1600s, 1890s, and 1970s and in the three-gauge HBR annual reconstruction during the 1650s and 1820s.

We produced a MJJAS seasonal streamflow reconstruction at the updated Partab Bridge record using PCR and BR (Figure 4). The final reconstruction produced by both methods (PCR and BR) are virtually identical, with only minor differences in the widths of their uncertainties (Figure S3). The reconstructions are highly correlated over the 575 years of reconstructed discharge (Pearson's  $r = 0.91$ ). Importantly, the calibration-validation statistics of the two reconstructions, as calculated using the CRSQ, VRSQ, CVRE, VRE, and VCE metrics, are comparable for the entire length of the reconstruction between 1430 and 2004 CE (Figure S4). The median values of these statistics for the full reconstructions are (i) CRSQ: PCR-49.80%, BR-56.04%; (ii) VRSQ: PCR-54.70%, BR-53.79%; (iii) CVRE: PCR-42.50%, BR-43.68%; (iv) VRE: PCR-0.52, BR-0.54; and (v) VCE: PCR-0.50, BR-0.52. The HBR model annual discharge estimates during the instrumental period are shown in Figure S5, and the calibration-validation statistics computed by LOOCV are shown in Figure S6. The consistently positive VRE and VCE values for each nest in PCR and BR reconstruction at Partab Bridge (Figure S4) and RE values for the HBR reconstructions at Doyian, Gilgit, and Kachora (Figure S6) indicate that reconstructions are skillful. Bayesian  $p$  values for predictions of the mean and mean squared errors were consistently close to or equal to 0.50 for all nests for the BR and HBR models.

#### 4.2. Climate Controls on Discharge

We then used the updated Partab Bridge (1962–2008 CE) record, the longest of our four records ( $n = 47$ ), to evaluate the relationship between climate and streamflow in the region. We first examined the relationship between monthly climate (precipitation and temperature) and mean MJJAS streamflow (Figure 6a) and tested for both contemporaneous and lagged relationships between climate and streamflow. All tests are based on the Pearson correlation and a two-sided hypothesis test with each series computed as first differences to minimize the effect of trends and autocorrelation in the data. We found MJJAS streamflow to be positively correlated with current year January through March precipitation ( $p < 0.01$ ), inversely correlated with prior year July ( $p < 0.05$ ), and positively correlated with current year June ( $p < 0.05$ ) and current year July ( $p < 0.01$ ) mean monthly temperature. When the same monthly climate versus discharge correlation analysis was carried out separately for each month of streamflow between May and September (not shown), we found that monthly discharge in a month was always significantly positively correlated with monthly temperature for that month ( $p < 0.01$ ). Based on these results, we infer the main climate seasons relevant for MJJAS streamflow at Partab Bridge to be January through March (JFM) precipitation likely in the form of snowfall, inferred from subfreezing temperatures in the region during this season (temperature boxplot Figure 3), along with MJJAS mean temperature.

Next, we computed spatial correlations between MJJAS discharge at Partab Bridge and JFM monthly mean precipitation and MJJAS monthly mean temperature to assess the spatial footprint of the climate to discharge relationship (Figures 6b and 6c). We found that MJJAS mean discharge at Partab Bridge is positively correlated (stippled blue shading for  $p < 0.01$ ) with JFM precipitation within the Karakoram region (Figure 6b)

and positively correlated with temperature (stippled red shading for  $\rho < 0.01$ ) over a broad spatial region spanning the Karakoram, Hindu Kush, and Toba Kakar ranges (Figure 6c). To further understand if the climate controls on discharge at Partab Bridge vary through the MJJAS season, we also computed the month-by-month correlations of mean May–July (MJJ) discharge against temperature and precipitation (Figure S7a), along with similar correlations for mean August–September discharge (Figure S7b). For MJJ discharge we find significant positive correlations with JFM precipitation and MJJ temperature ( $\rho < 0.05$ ), while for August–September discharge significant positive correlations were found with January and March precipitation and August temperature ( $\rho < 0.01$ ).

We also performed a similar month-by-month correlation analysis between climate variables and mean MJJAS flow at Doyian ( $n = 35$ ), Gilgit ( $n = 27$ ), and Kachora ( $n = 38$ ) (Figure S8). Discharge at all gauges shows a significant positive correlation with February precipitation ( $\rho < 0.01$ ). At Doyian there is a broad significant positive correlation between discharge and February through May precipitation ( $\rho < 0.05$ ), but no significant correlation between discharge and temperature was observed (Figure S8a). At Gilgit, discharge was found to be positively correlated with February and March precipitation ( $\rho < 0.05$ ), and negatively correlated with February temperature ( $\rho < 0.05$ ; Figure S8b). Finally, at Kachora discharge was significantly positively correlated with JFM precipitation ( $\rho < 0.01$ ) and with May, June, and August temperature (Figure S8c). While the HBR reconstructions at Doyian, Gilgit, and Kachora presented in the previous section are for mean annual discharge, we found that climate to streamflow relationship was nearly identical for mean annual discharge and mean MJJAS discharge shown in Figure S8 (not shown).

The positive relationship between wintertime precipitation and summertime temperature at Partab Bridge and Kachora suggests that discharge at these gauges is influenced by both winter snow accumulation and summer snow and glacial melt. However, at Doyian and Gilgit the lack of temperature sensitivity suggests that discharge at these gauges depends primarily on wintertime snowfall and with temperature-dependent glacial melt playing little to no contributing role. These findings are consistent with Mukhopadhyay and Khan (2014), who use the percentage of watershed within a hypsometric band (i.e., elevation zone) and determine that main Indus sub-basins where Kachora and Partab Bridge are located are more heavily glaciated and have a higher mean elevation than the Astore and Gilgit sub-basins where the Doyian and Gilgit gauging stations are located (also see Table 1 for basin names).

### 4.3. Climate Controls on Tree Growth

We then examined the climate to tree growth response of the predictor suite used in the first nest for the MJJAS reconstruction at Partab Bridge. In our reconstruction model, we retained the first four PC time series in the first nest, with the following percentage variance explained, PC1-50%, PC2-14%, PC3-9%, and PC4-7%. Cumulatively, these PCs explain 80% to the total variance of the predictor suite. The month-by-month climate to PC1 and PC2 correlations for the time period 1962–2008 is shown in Figures 7a and 7b, while those for PC3 and PC4 are shown in Figures S7c and S7d. We find that PC1 shows a broad January through May positive correlation with precipitation ( $\rho < 0.01$ ), while PC2 shows a significant inverse correlation with temperature that peaks in current year May through August ( $\rho < 0.01$ ). Both PC3 and PC4 show significant inverse correlations with June ( $\rho < 0.01$ ) and July ( $\rho < 0.05$ ) temperature. The PC loadings of each tree ring series on the first four PC time series are shown in Figure 7c. All sites except MuaABP.t1 and NltPCS.t1 show strong positive loadings on PC1, as indicated by the shaded green circles. This, together with Figure 7a, reveals that almost all tree ring predictors used in our model respond positively to wintertime snowfall. While the PC2–PC4 time series all represent an inverse summer temperature sensitivity, the loadings of each tree ring series was either positive (green shading) or negative (pink shading). A positive loading on PC2–PC4 indicates that a particular tree ring series responds inversely to summer temperature, while a negative loading indicates that the tree ring site responds positively to summer temperature (also see Ahmed et al., 2011). We also conducted a similar analysis with the first four PC time series with eigenvalues greater than one that were retained as predictors in the first nest for the HBR reconstruction at Doyian, Gilgit, and Kachora. The PCs showed a nearly identical climate response as the first four PCs retained in the BR model at Partab Bridge (not shown).

### 4.4. Climate Informed Discharge Prediction at Partab Bridge

To test if anomalies in winter precipitation and summer temperature can explain the 1990s high flow (Figures 4 and 5), we developed a multivariate regression model to predict MJJAS mean streamflow at

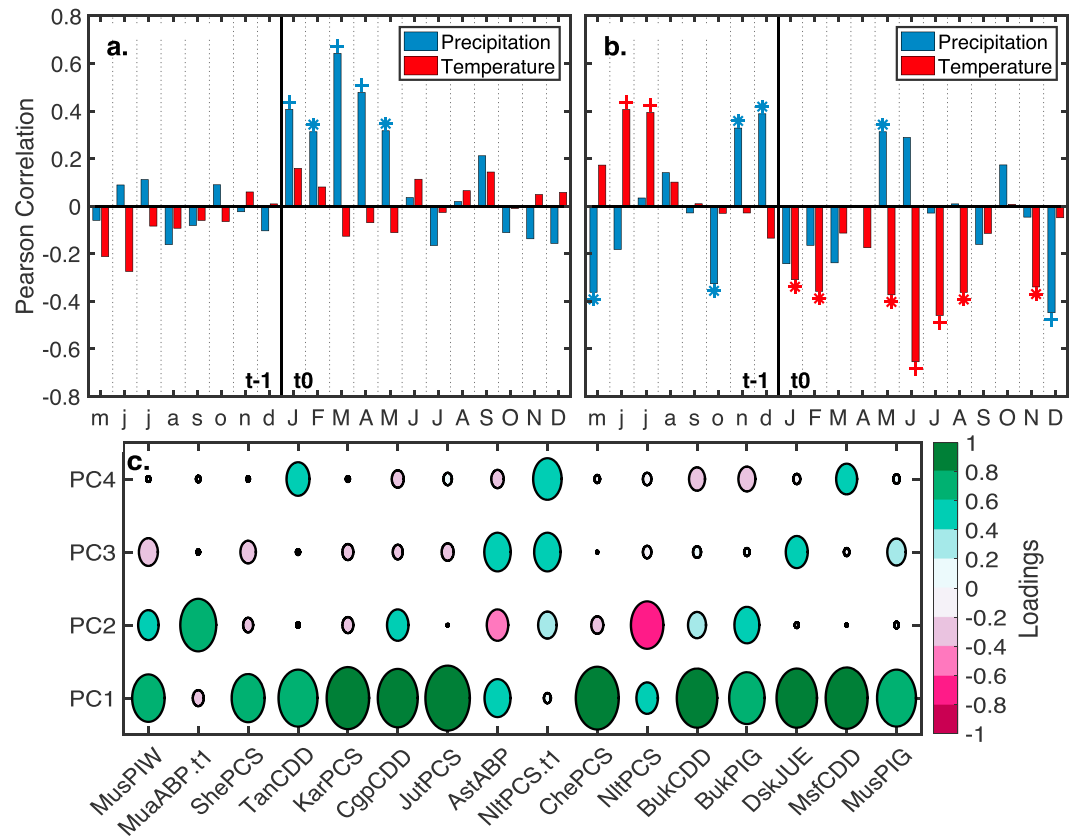


**Figure 7.** Climate response during instrumental period of the tree ring predictor suite of the first nest between 1962 and 2004. (a) Same as Figure 5a but for PC1 time series and (b) PC2 time series. (c) Loadings of each tree ring series on PC1 through PC4 used in the Model I at Partab Bridge with the size of the circle and its shading are scaled to magnitude of loading on the respective PC. PC = principal component.

Partab Bridge using JFM mean precipitation and MJJAS mean temperature as predictors (green line, Figure 8). The multivariate regression model was built using the raw (i.e., not first differenced) climate data and BR with LOOCV. This climate-informed statistical streamflow model explained ~49.34% of the variance in the instrumental data. This climate-based streamflow prediction of instrumental MJJAS discharge at Partab Bridge was compared to that predicted by the PCR and BR reconstructions (red and blue lines in Figure 8).

The PCR and BR model estimates are significantly correlated at  $r = 0.98$  during the instrumental period between 1962 and 2004, and these modes each explained 52.97% and 54.43% of the variance in the instrumental data. The calibration and validation statistics of the climate-informed statistical streamflow model as measured by the CRSQ, CVRE, and RE metrics for the model are presented in Figure S9. Using this model, we present discharge estimates of streamflow for the period between 2009 and 2016 beyond the last year of instrumental data that ends in 2008 (Figure 8). While the climate-based model predicts the high flow in 1973 reasonably well, a year of significant UIB flooding (Deutsch & Ruggles, 1978), it underpredicts flow between 1991 and 2000 while still capturing the direction of interannual variability during this period. During the common period of overlap between 1962 and 2008 the RMSEs of the BR, PCR, and climate-variable informed statistical models are 370.93  $m^3/s$ , 373.58  $m^3/s$ , and 421.13  $m^3/s$ , respectively, while the median-normalized RMSEs are 10.19%, 10.26%, and 11.57%, respectively.

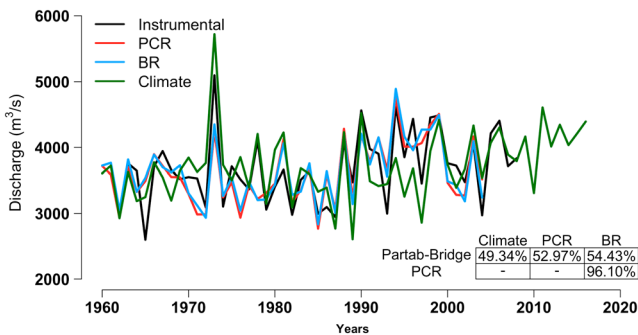


**Figure 8.** Instrumental mean MJJAS discharge at Partab Bridge (black) compared against predictions of flow ( $m^3/s$ ) generated by models using PCR (red), BR (blue), and climate variables (green). Table shows  $R^2$  across instrumental data and models. MJJAS = May–September; PCR = principal components regression; BR = Bayesian regression.

However, for the period of high flow between 1991 and 2000 the RMSE for the three models are 397.17 m<sup>3</sup>/s, 351.75 m<sup>3</sup>/s, and 532.52 m<sup>3</sup>/s, respectively, while the median-normalized RMSEs are 10.08%, 8.93%, and 13.52%. The greatly increased RMSE and median-normalized RMSE for the climate-variable informed model between 1991 and 2000 as compared to 1962–2004 indicate that the climate-informed statistical model is performing relatively poorly in this decade compared to its quality of fit over the entire instrumental period.

## 5. Discussion and Conclusions

Understanding climate change and assessing recent trends in climate data require an understanding of long-term natural variability. For the UIB, available instrumental streamflow data only span two to four decades, an insufficient time span to accurately characterize decadal to centennial time scale streamflow variability. Paleohydrologic records can play an important role in helping us extend the instrumental record to better understand these longer-term processes (e.g., Pages Hydro2k Consortium, 2017; Stockton & Jacoby, 1976). Our reconstructions of past discharge at four gauging stations (Partab Bridge, Doyian, Gilgit, and Kachora) extend our instrumental record of UIB discharge back six centuries to the 1400s. Our reconstructions highlight extended dry periods during the mid-1600s, late 1700s, and early 1900s that have no analog in the short instrumental period (Figures 4 and 5, also see Cook et al., 2013). Further, these longer-term reconstructions of flow help us better contextualize streamflow variability during the past two decades associated with the *Karakoram Anomaly* (Forsythe et al., 2017; Hewitt, 2005). The high flows in the instrumental period in the late 1980s through 1990s do appear to be unusual in the context of the past six centuries. Using the reconstructions as a reference baseline, the recent post-2000 decrease in discharge (Archer et al., 2010) may represent a return to long-term mean flow conditions following the high discharge rates observed in the 1990s. At the same time, our climate-variable informed discharge predictions between 2009 and 2016 at Partab Bridge (Figure 8) suggest that discharge rates might be increasing after the decrease between 2000 and 2009 due to rising summer temperatures. However, considering the underperformance of the climate-informed model in the 1990s, this result should be viewed with caution.

This most recent wet period, however, is difficult to reconcile with the main climate drivers of discharge in the region. Nevertheless, the high flow between 1991 and 2000 likely has climatic origins. We infer this because the tree ring-based models are able to capture the high instrumental discharge during this period. However, its proximate causes are likely not changes in JFM snowfall or summer MJJAS temperatures. This is shown by the much better prediction of high streamflow between 1991 and 2000 by the two tree ring models (BR and PCR) as compared to the climate-informed model, even though all three models exhibit similar overall performance for the entire instrumental period between 1962 and 2004. Specifically, the climate variable-informed statistical model has a large offset in the magnitude of predicted discharge during this period despite capturing the direction of interannual variability. Although the underlying causes of this wet period still need to be investigated, they may lie in climate variability in the shoulder seasons that may be still relevant to streamflow yet not be primary controls on the interannual variability of streamflow. The reason our tree ring model captures some of these changes may be because the tree growth to climate response exhibits a slightly broader climate sensitivity than the streamflow data. When analyzing the instrumental precipitation and temperature data, we did not find any significant changes in monthly climate (e.g., summer precipitation) during this period. However, most of the climate records used in our discharge model come from low-elevation locations relative to the high-elevation runoff generating regions of the UIB. It is possible that some of the poorer discharge estimates may be a reflection of this. These low-elevation stations might not be capturing regional processes that might differentially affect high- and low-elevation regions, such as a preferential increase in high-elevation winter snowfall (Kapnick et al., 2014), or land surface feedbacks from lowland irrigation causing high-elevation snowfall (de Kok et al., 2018).

Over the coming few decades, discharge in the UIB is expected to increase based on climate model predictions due to a combination of predicted warming enhancing the rate of glacial melt and increases in winter and summer precipitation (Ali et al., 2015; Brun et al., 2017; Immerzeel et al., 2013; Kraaijenbrink et al., 2017; Lutz et al., 2014; Wijngaard et al., 2017). At the subregional level, however, these changes might not be uniform. For example, the climatic controls of MJJAS discharge at Partab Bridge and Kachora are primarily wintertime (JFM) snowfall and summertime temperature, but at Doyian and Gilgit there is no temperature dependence of streamflow. Consequently, in basins where glacial melt is important (Partab Bridge and

Kachora), future warming may increase discharge as long as the remaining glacial mass can support increased flow. Assuming no increase in wintertime snowfall to offset the loss of glacier ice, this meltwater contribution to streamflow will very likely decrease sometime in the future, thus leading to a long-term decrease in discharge. In snowfall-dominated sub-basins (Doyian and Gilgit) changes in streamflow are more likely to depend on changes in wintertime snowfall. At no gauge did we find a relationship between peak flow MJJAS season discharge and summertime monsoonal precipitation. This suggests that while monsoonal precipitation may play a minor contributing role in maintaining baseline flow (Mukhopadhyay & Khan, 2014), it is not a driver of interannual discharge variability. The spatial correlation between MJJAS flow at Partab Bridge and JFM winter precipitation shows a region of positive correlation that is relatively limited to Karakoram, Hindu Kush, and Western Himalaya. This region of positive correlations broadly spans the region where winter is the most important precipitation season (Greene & Robertson, 2017; Kapnick et al., 2014). The region of significant positive temperature correlations with discharge extends west and southwest from the Karakoram broadly tracing the region of the Pakistan-Afghanistan border and does not extend east into the main Himalayas (Figure 6c). This suggests that the atmospheric processes that control temperature-driven glacial melt in the summer are different for the Karakoram and the main Himalayas, consistent with the findings of Forsythe et al. (2017, their Figure 2), hypothesized by them to be the position of the summertime westerly jet.

We establish that tree ring reconstruction of past MJJAS discharge at Partab Bridge produced using PCR and BR is nearly identical in terms of the median flow reconstructed for each year. While there are differences in the widths of the uncertainties, produced by the two reconstructions, estimated from regression prediction intervals and Bayesian credible intervals, respectively, these differences in uncertainties appear to be minor. We find that BR typically, but not always, produces slightly wider uncertainty intervals. Commonly used statistical approaches for tree ring reconstructions of past streamflow and climate include PCR (e.g., Allen et al., 2018; Anchukaitis et al., 2017; Cook et al., 2010, 1999, 2013; Palmer et al., 2015; Stahle et al., 2016), a Bayesian framework (Devineni et al., 2013; Luterbacher et al., 2016; Steinschneider et al., 2017; Tingley & Huybers, 2010), along with other statistical methods (e.g., Bracken et al., 2016; Gangopadhyay et al., 2009; Woodhouse et al., 2016). Our results suggest that for a one predictand variable case at the Partab Bridge gauge, both PCR and BR methods produce comparable reconstructions in terms of their estimates, uncertainties, and reconstruction skill statistics. However, for a multiple-gauge network within a watershed, HBR with partial pooling provides a powerful framework to develop reconstructions of streamflow (or climate) with short instrumental records and missing data. This finding was also supported by our preliminary analysis (not presented here), where we found that our HBR model with partial pooling performed better than alternate HBR models with *no pooling* and *full pooling* (also see Devineni et al., 2013). Finally, we also demonstrate that the suite of tree ring predictors used in the reconstructions have a nearly identical climate to growth response as the climate to streamflow relationship. This enhances our confidence that the reconstructions presented here capture paleo-hydrologic variability caused by past changes in these climate variables, and that these reconstructions help us better characterize longer-term climate-driven decadal to centennial time scale streamflow variability within the UIB.

#### Acknowledgments

M. P. R. is grateful to funding from the Lamont Climate Center and Chevron Student Initiative Fund and thanks the Past Global Changes Paleo-Floods Working Group and Balaji Rajagopalan (CU Boulder) for helpful feedback and suggestions on the manuscript. Authors acknowledge support from the NSF AGS 0402474 and U.S. Agency for International Development (USAID) NAS Grant PGA-P280423 for the original development of the tree ring data sets used. The authors declare no conflict(s) of interest. Data set access - CRU TS v.4.01: <https://crudata.uea.ac.uk/cru/data/hrg/>; tree ring data: <https://www.ncdc.noaa.gov/data-access/paleoclimatology-data/datasets/tree-ring>; streamflow discharge data and reconstructions: supporting information Data S1; and JAGS code: supporting information Data S2. Lamont contribution 8232.

#### References

- Ahmed, M., Palmer, J., Khan, N., Wahab, M., Fenwick, P., Esper, J., & Cook, E. (2011). The dendroclimatic potential of conifers from northern Pakistan. *Dendrochronologia*, 29(2), 77–88. <https://doi.org/10.1016/j.dendro.2010.08.007>
- Ahmed, M., Zafar, M. U., Hussain, A., Akbar, M., Wahab, M., & Khan, N. (2013). Dendroclimatic and dendrohydrological response of two tree species from Gilgit valleys. *Pakistan Journal of Botany*, 45, 987–992.
- Ali, S., Li, D., Congbin, F., & Khan, F. (2015). Twenty first century climatic and hydrological changes over Upper Indus Basin of Himalayan region of Pakistan. *Environmental Research Letters*, 10(1), 014007. <https://doi.org/10.1088/1748-9326/10/1/014007>
- Allen, K. J., Cook, E. R., Evans, R., Francey, R., Buckley, B. M., Palmer, J. G., et al. (2018). Lack of cool, not warm, extremes distinguishes late 20th Century climate in 979-year Tasmanian summer temperature reconstruction. *Environmental Research Letters*, 13(3), 034041.
- Anchukaitis, K. J., Wilson, R., Briffa, K. R., Büntgen, U., Cook, E. R., D'Arrigo, R., et al. (2017). Last millennium Northern Hemisphere summer temperatures from tree rings: Part II, spatially resolved reconstructions. *Quaternary Science Reviews*, 163, 1–22. <https://doi.org/10.1016/j.quascirev.2017.02.020>
- Archer, D. R. (2003). Contrasting hydrological regimes in the Upper Indus Basin. *Journal of Hydrology*, 274(1–4), 198–210. [https://doi.org/10.1016/S0022-1694\(02\)00414-6](https://doi.org/10.1016/S0022-1694(02)00414-6)
- Archer, D. R., Forsythe, N., Fowler, H. J., & Shah, S. M. (2010). Sustainability of water resources management in the Indus Basin under changing climatic and socio economic conditions. *Hydrology and Earth System Sciences*, 14(8), 1669–1680. <https://doi.org/10.5194/hess-14-1669-2010>

- Bashir, F., Zeng, X., Gupta, H., & Hazenberg, P. (2017). A hydrometeorological perspective on the Karakoram anomaly using unique valley-based synoptic weather observations. *Geophysical Research Letters*, *44*, 10,470–10,478. <https://doi.org/10.1002/2017GL075284>
- Benn, D., & Owen, L. (1998). The role of the Indian summer monsoon and the mid-latitude westerlies in Himalayan glaciation: Review and speculative discussion. *Journal of the Geological Society*, *155*(2), 353–363. <https://doi.org/10.1144/gsjgs.155.2.0353>
- Bolch, T., Kulkarni, A., Kääb, A., Huggel, C., Paul, F., Cogley, J. G., et al. (2012). The state and fate of Himalayan glaciers. *Science*, *336*(6079), 310–314. <https://doi.org/10.1126/science.1215828>
- Bracken, C., Rajagopalan, B., & Woodhouse, C. A. (2016). A Bayesian hierarchical nonhomogeneous hidden Markov model for multisite streamflow reconstructions. *Water Resources Research*, *52*, 7837–7850. <https://doi.org/10.1002/2016WR018887>
- Brun, F., Berthier, E., Wagnon, P., Kääb, A., & Treichler, D. (2017). A spatially resolved estimate of High Mountain Asia glacier mass balances from 2000 to 2016. *Nature Geoscience*, *10*(9), 668–673. <https://doi.org/10.1038/ngeo2999>
- Bunn, A. G. (2010). Statistical and visual cross dating in R using the dplR library. *Dendrochronologia*, *28*(4), 251–258. <https://doi.org/10.1016/j.dendro.2009.12.001>
- Cook, E. R., Anchukaitis, K. J., Buckley, B. M., D'Arrigo, R. D., Jacoby, G. C., & Wright, W. E. (2010). Asian monsoon failure and megadrought during the last millennium. *Science*, *328*(5977), 486–489. <https://doi.org/10.1126/science.1185188>
- Cook, E. R., & Jacoby, G. C. (1983). Potomac River streamflow since 1730 as reconstructed by tree rings. *Journal of Climate and Applied Meteorology*, *22*(10), 1659–1672. [https://doi.org/10.1175/1520-0450\(1983\)022<1659:prssar>2.0.co;2](https://doi.org/10.1175/1520-0450(1983)022<1659:prssar>2.0.co;2)
- Cook, E. R., & Kairiukstis, L. (1990). *Methods of dendrochronology: Applications in the environmental sciences*. Dordrecht, Netherlands: Kluwer.
- Cook, E. R., Meko, D. M., Stahle, D. W., & Cleaveland, M. K. (1999). Drought reconstructions for the continental United States. *Journal of Climate*, *12*(4), 1145–1162. [https://doi.org/10.1175/1520-0442\(1999\)012<1145:drftcu>2.0.co;2](https://doi.org/10.1175/1520-0442(1999)012<1145:drftcu>2.0.co;2)
- Cook, E. R., Palmer, J. G., Ahmed, M., Woodhouse, C. A., Fenwick, P., Zafar, M. U., et al. (2013). Five centuries of Upper Indus River flow from tree rings. *Journal of Hydrology*, *486*, 365–375. <https://doi.org/10.1016/j.jhydrol.2013.02.004>
- Cooley, W. W., & Lohnes, P. R. (1971). *Multivariate data analysis*. New York: John Wiley.
- D'Arrigo, R., Abram, N., Ummenhofer, C., Palmer, J., & Mudelsee, M. (2011). Reconstructed streamflow for Citarum River, Java, Indonesia: Linkages to tropical climate dynamics. *Climate Dynamics*, *36*(3–4), 451–462. <https://doi.org/10.1007/s00382-009-0717-2>
- de Kok, R. J., Tuinenburg, O. A., Bonekamp, P. N. J., & Immerzeel, W. W. (2018). Irrigation as a potential driver for anomalous glacier behaviour in High Mountain Asia. *Geophysical Research Letters*, *45*, 2047–2054. <https://doi.org/10.1002/2017GL076158>
- Deutsch, M., & Ruggles, F. H. (1978). Hydrological applications of Landsat Imagery used in the study of the 1973 Indus River flood, Pakistan. *JAWRA Journal of the American Water Resources Association*, *14*(2), 261–274. <https://doi.org/10.1111/j.1752-1688.1978.tb02165.x>
- Devineni, N., Lall, U., Pederson, N., & Cook, E. (2013). A tree-ring-based reconstruction of Delaware River basin streamflow using hierarchical Bayesian regression. *Journal of Climate*, *26*(12), 4357–4374. <https://doi.org/10.1175/jcli-d-11-00675.1>
- Farhan, S. B., Zhang, Y., Ma, Y., Guo, Y., & Ma, N. (2015). Hydrological regimes under the conjunction of westerly and monsoon climates: a case investigation in the Astore Basin, Northwestern Himalaya. *Climate Dynamics*, *44*(11), 3015–3032. <https://doi.org/10.1007/s00382-014-2409-9>
- Forsythe, N., Fowler, H. J., Li, X.-F., Blenkinsop, S., & Pritchard, D. (2017). Karakoram temperature and glacial melt driven by regional atmospheric circulation variability. *Nature Climate Change*, *7*(9), 664–670. <https://doi.org/10.1038/nclimate3361>
- Fowler, H., & Archer, D. (2006). Conflicting signals of climatic change in the Upper Indus Basin. *Journal of Climate*, *19*(17), 4276–4293. <https://doi.org/10.1175/JCLI3860.1>
- Fritts, H. (1976). *Tree rings and climate* (p. 567). San Diego, CA: Academic.
- Gangopadhyay, S., Harding, B. L., Rajagopalan, B., Lukas, J. J., & Fulp, T. J. (2009). A nonparametric approach for paleohydrologic reconstruction of annual streamflow ensembles. *Water Resources Research*, *45*, W06417. <https://doi.org/10.1029/2008WR007201>
- Gardelle, J., Berthier, E., & Arnaud, Y. (2012). Slight mass gain of Karakoram glaciers in the early twenty-first century. *Nature Geoscience*, *5*(5), 322–325. <https://doi.org/10.1038/ngeo1450>
- Gelman, A., & Hill, J. (2006). *Data analysis using regression and multilevel/hierarchical models*. New York: Cambridge University Press. <https://doi.org/10.1017/CBO9780511790942>
- Gelman, A., & Rubin, D. B. (1992). Inference from iterative simulation using multiple sequences. *Statistical Science*, *7*(4), 457–472. <https://doi.org/10.1214/ss/1177011136>
- Greene, A. M., & Robertson, A. W. (2017). Interannual and low-frequency variability of Upper Indus Basin winter/spring precipitation in observations and CMIP5 models. *Climate Dynamics*, *49*(11–12), 4171–4188. <https://doi.org/10.1007/s00382-017-3571-7>
- Guttman, L. (1954). Some necessary conditions for common-factor analysis. *Psychometrika*, *19*(2), 149–161. <https://doi.org/10.1007/bf02289162>
- Harley, G. L., & Maxwell, J. T. (2017). Current declines of Pecos River (New Mexico, USA) streamflow in a 700-year context. *The Holocene*, *28*(5), 767–777. <https://doi.org/10.1177/0959683617744263>
- Harley, G. L., Maxwell, J. T., Larson, E., Grissino-Mayer, H. D., Henderson, J., & Huffman, J. (2017). Suwannee River flow variability 1550–2005 CE reconstructed from a multispecies tree-ring network. *Journal of Hydrology*, *544*, 438–451. <https://doi.org/10.1016/j.jhydrol.2016.11.020>
- Harpold, A. A., & Brooks, P. D. (2018). Humidity determines snowpack ablation under a warming climate. *Proceedings of the National Academy of Sciences*, *115*(6), 1215–1220. <https://doi.org/10.1073/pnas.1716789115>
- Hasson, S., Böhner, J., & Lucarini, V. (2017). Prevailing climatic trends and runoff response from Hindukush–Karakoram–Himalaya, Upper Indus Basin. *Earth System Dynamics*, *8*(2), 337–355. <https://doi.org/10.5194/esd-8-337-2017>
- Hewitt, K. (2005). The Karakoram anomaly? Glacier expansion and the 'elevation effect,' Karakoram Himalaya. *Mountain Research and Development*, *25*(4), 332–340. [https://doi.org/10.1659/0276-4741\(2005\)025\[0332:TKAGEA\]2.0.CO;2](https://doi.org/10.1659/0276-4741(2005)025[0332:TKAGEA]2.0.CO;2)
- Ho, M., Lall, U., Sun, X., & Cook, E. R. (2017). Multiscale temporal variability and regional patterns in 555 years of conterminous U.S. streamflow. *Water Resources Research*, *53*, 3047–3066. <https://doi.org/10.1002/2016WR019632>
- Huss, M., & Hock, R. (2018). Global-scale hydrological response to future glacier mass loss. *Nature Climate Change*, *8*(2), 135–140. <https://doi.org/10.1038/s41558-017-0049-x>
- Immerzeel, W. W., Droogers, P., de Jong, S. M., & Bierkens, M. F. P. (2009). Large-scale monitoring of snow cover and runoff simulation in Himalayan river basins using remote sensing. *Remote Sensing of Environment*, *113*(1), 40–49. <https://doi.org/10.1016/j.rse.2008.08.010>
- Immerzeel, W. W., Pellicciotti, F., & Bierkens, M. F. P. (2013). Rising river flows throughout the twenty-first century in two Himalayan glacierized watersheds. *Nature Geoscience*, *6*(9), 742–745. <https://doi.org/10.1038/ngeo1896>
- Immerzeel, W. W., van Beek, L. P. H., & Bierkens, M. F. P. (2010). Climate change will affect the Asian water towers. *Science*, *328*(5984), 1382–1385. <https://doi.org/10.1126/science.1183188>
- Janssen, P. H. M., & Heuberger, P. S. C. (1995). Calibration of process-oriented models. *Ecological Modelling*, *83*(1–2), 55–66. [https://doi.org/10.1016/0304-3800\(95\)00084-9](https://doi.org/10.1016/0304-3800(95)00084-9)
- Kaiser, H. F. (1960). The application of electronic computers to factor analysis. *Educational and Psychological Measurement*, *20*(1), 141–151. <https://doi.org/10.1177/001316446002000116>

- Kapnick, S. B., Delworth, T. L., Ashfaq, M., Malyshev, S., & Milly, P. C. D. (2014). Snowfall less sensitive to warming in Karakoram than in Himalayas due to a unique seasonal cycle. *Nature Geoscience*, *7*(11), 834–840. <https://doi.org/10.1038/ngeo2269>
- Kraaijenbrink, P. D. A., Bierkens, M. F. P., Lutz, A. F., & Immerzeel, W. W. (2017). Impact of a global temperature rise of 1.5 degrees Celsius on Asia's glaciers. *Nature*, *549*, 257. <https://doi.org/10.1038/nature23878>
- Luterbacher, J., Werner, J. P., Smerdon, J. E., Fernández-Donado, L., González-Rouco, F. J., Barriopedro, D., et al. (2016). European summer temperatures since Roman times. *Environmental Research Letters*, *11*(2), 024001. <https://doi.org/10.1088/1748-9326/11/2/024001>
- Lutz, A. F., Immerzeel, W., Kraaijenbrink, P., Shrestha, A. B., & Bierkens, M. F. (2016). Climate change impacts on the upper Indus hydrology: Sources, shifts and extremes. *PLoS One*, *11*(11), e0165630. <https://doi.org/10.1371/journal.pone.0165630>
- Lutz, A. F., Immerzeel, W. W., Shrestha, A. B., & Bierkens, M. F. P. (2014). Consistent increase in high Asia's runoff due to increasing glacier melt and precipitation. *Nature Climate Change*, *4*(7), 587–592. <https://doi.org/10.1038/nclimate2237>
- Meko, D. M. (1997). Dendroclimatic reconstruction with time varying predictor subsets of tree indices. *Journal of Climate*, *10*(4), 687–696. [https://doi.org/10.1175/1520-0442\(1997\)010<0687:Drwtvp>2.0.Co;2](https://doi.org/10.1175/1520-0442(1997)010<0687:Drwtvp>2.0.Co;2)
- Meko, D. M. (2006). Tree-ring inferences on water-level fluctuations of Lake Athabasca. *Canadian Water Resources Journal/Revue canadienne des ressources hydriques*, *31*(4), 229–248. <https://doi.org/10.4296/cwrj3104229>
- Meko, D. M., Stockton, C. W., & Boggess, W. R. (1995). The tree-ring record of severe sustained drought. *JAWRA Journal of the American Water Resources Association*, *31*(5), 789–801. <https://doi.org/10.1111/j.1752-1688.1995.tb03401.x>
- Meko, D. M., & Woodhouse, C. A. (2011). Application of streamflow reconstruction to water resources management. In M. K. Hughes, T. W. Swetnam, & H. F. Diaz (Eds.), *Dendroclimatology: Progress and Prospects* (pp. 231–261). Dordrecht, Netherlands: Springer. [https://doi.org/10.1007/978-1-4020-5725-0\\_8](https://doi.org/10.1007/978-1-4020-5725-0_8)
- Melvin, T. M., & Briffa, K. R. (2008). A “signal-free” approach to dendroclimatic standardisation. *Dendrochronologia*, *26*(2), 71–86. <https://doi.org/10.1016/j.dendro.2007.12.001>
- Minora, U., Bocchiola, D., D'Agata, C., Maragno, D., Mayer, C., Lambrecht, A., et al. (2013). 2001–2010 glacier changes in the Central Karakoram National Park: A contribution to evaluate the magnitude and rate of the “Karakoram anomaly”. *The Cryosphere Discussions*, *7*(3), 2891–2941. <https://doi.org/10.5194/tcd-7-2891-2013>
- Mukhopadhyay, B., & Khan, A. (2014). A quantitative assessment of the genetic sources of the hydrologic flow regimes in Upper Indus Basin and its significance in a changing climate. *Journal of Hydrology*, *509*, 549–572. <https://doi.org/10.1016/j.jhydrol.2013.11.059>
- Nash, J. E., & Sutcliffe, J. V. (1970). River flow forecasting through conceptual models part I—A discussion of principles. *Journal of Hydrology*, *10*(3), 282–290. [https://doi.org/10.1016/0022-1694\(70\)90255-6](https://doi.org/10.1016/0022-1694(70)90255-6)
- Pages Hydro2k Consortium (2017). Comparing proxy and model estimates of hydroclimate variability and change over the Common Era. *Climate of the Past*, *13*(12), 1851–1900. <https://doi.org/10.5194/cp-13-1851-2017>
- Palazzi, E., von Hardenberg, J., Terzago, S., & Provenzale, A. (2015). Precipitation in the Karakoram-Himalaya: a CIMP5 view. *Climate Dynamics*, *45*(1), 21–45. <https://doi.org/10.1007/s00382-014-2341-z>
- Palmer, J. G., Cook, E. R., Turney, C. S., Allen, K., Fenwick, P., Cook, B. I., et al. (2015). Drought variability in the eastern Australia and New Zealand summer drought atlas (ANZDA, CE 1500–2012) modulated by the Interdecadal Pacific Oscillation. *Environmental Research Letters*, *10*(12), 124002. <https://doi.org/10.1088/1748-9326/10/12/124002>
- Plummer, M. (2003). JAGS: A program for analysis of Bayesian graphical models using Gibbs sampling. Paper presented at the proceedings of the 3rd international workshop on distributed statistical computing.
- Rashid, M. U., Latif, A., & Azmat, M. (2018). Optimizing irrigation deficit of multipurpose Cascade reservoirs. *Water Resources Management*, *32*, 1675–1687. <https://doi.org/10.1007/s11269-017-1897-x>
- Ridley, J., Wiltshire, A., & Mathison, C. (2013). More frequent occurrence of westerly disturbances in Karakoram up to 2100. *Science of the Total Environment*, *468*, S31–S35.
- Shapiro, S. S., & Wilk, M. B. (1965). An analysis of variance test for normality (complete samples). *Biometrika*, *52*(3–4), 591–611. <https://doi.org/10.1093/biomet/52.3-4.591>
- Stahle, D. W., Cook, E. R., Burnette, D. J., Villanueva, J., Cerano, J., Burns, J. N., et al. (2016). The Mexican Drought Atlas: Tree-ring reconstructions of the soil moisture balance during the late pre-Hispanic, colonial, and modern eras. *Quaternary Science Reviews*, *149*, 34–60. <https://doi.org/10.1016/j.quascirev.2016.06.018>
- Steinschneider, S., Cook, E. R., Briffa, K. R., & Lall, U. (2017). Hierarchical regression models for dendroclimatic standardization and climate reconstruction. *Dendrochronologia*, *44*, 174–186. <https://doi.org/10.1016/j.dendro.2017.05.003>
- Stockton, C., & Jacoby, G. C. (1976). Long-term surface-water supply and streamflow trends in the upper Colorado River basin. *Lake Powell Research Project Bulletin*, *18*, 70.
- Tahir, A. A., Chevallier, P., Arnaud, Y., Neppel, L., & Ahmad, B. (2011). Modeling snowmelt-runoff under climate scenarios in the Hunza River basin, Karakoram range, northern Pakistan. *Journal of Hydrology*, *409*(1–2), 104–117. <https://doi.org/10.1016/j.jhydrol.2011.08.035>
- Tingley, M. P., & Huybers, P. (2010). A Bayesian algorithm for reconstructing climate anomalies in space and time. Part II: Comparison with the regularized expectation–maximization algorithm. *Journal of Climate*, *23*(10), 2782–2800. <https://doi.org/10.1175/2009jcli3016.1>
- Vinod, H. (2006). Maximum entropy ensembles for time series inference in economics. *Journal of Asian Economics*, *17*(6), 955–978. <https://doi.org/10.1016/j.asieco.2006.09.001>
- Vinod, H., & López-de-Lacalle, J. (2009). Maximum entropy bootstrap for time series: The meboot R package. *Journal of Statistical Software*, *29*(5). <https://doi.org/10.18637/jss.v029.i05>
- Wijngaard, R. R., Lutz, A. F., Nepal, S., Khanal, S., Pradhananga, S., Shrestha, A. B., & Immerzeel, W. W. (2017). Future changes in hydro-climatic extremes in the upper Indus, Ganges, and Brahmaputra River basins. *PLoS One*, *12*(12), e0190224. <https://doi.org/10.1371/journal.pone.0190224>
- Woodhouse, C. A., Lukas, J., Morino, K., Meko, D. M., & Hirschboeck, K. K. (2016). Using the past to plan for the future? The value of paleoclimate reconstructions for water resource planning. In *Water Policy and Planning in a Variable and Changing Climate* (161–182). Boca Raton, FL.
- Woodhouse, C. A., & Lukas, J. J. (2006). Multi-century tree-ring reconstructions of Colorado streamflow for water resource planning. *Climatic Change*, *78*(2–4), 293–315. <https://doi.org/10.1007/s10584-006-9055-0>
- Zafar, M. U., Ahmed, M., Farooq, M. A., Akbar, M., & Hussain, A. (2010). Standardized tree ring chronologies of *Picea smithiana* from two new sites of northern area Pakistan. *World Applied Sciences Journal*, *11*(12), 1531–1536.
- Zafar, M. U., Ahmed, M., Rao, M. P., Buckley, B. M., Khan, N., Wahab, M., & Palmer, J. (2015). Karakoram temperature out of phase with hemispheric trends for the past five centuries. *Climate Dynamics*, *46*(5–6), 1943–1952. <https://doi.org/10.1007/s00382-015-2685-z>
- Zawahri, N. A. (2009). India, Pakistan and cooperation along the Indus River system. *Water Policy*, *11*(1), 1–20. <https://doi.org/10.2166/wp.2009.010>